

## Article

# Combining Artificial Neural Network and Seeker Optimization Algorithm for Predicting Compression Capacity of Concrete-Filled Steel Tube Columns

Pan Hu <sup>1,2</sup>, Hamidreza Aghajaninefah <sup>3</sup>, Arsalan Anvari <sup>4</sup> and Moncef L. Nehdi <sup>5,\*</sup> <sup>1</sup> School of Civil and Architectural Engineering, Technical University of Munich, 80333 Munich, Germany<sup>2</sup> Wuhan Municipal Construction Group Co., Ltd., Wuhan 430023, China<sup>3</sup> Department of Civil Engineering, Faculty of Engineering, Qazvin Branch Islamic Azad University, Qazvin 3419915195, Iran<sup>4</sup> Engineering and Management, Faculty of Civil Engineering, Science and Research Branch, Islamic Azad University, Tehran 1477893855, Iran<sup>5</sup> Department of Civil Engineering, McMaster University, Hamilton, ON L8S 4L8, Canada

\* Correspondence: nehdim@mcmaster.ca

**Abstract:** Accurate and reliable estimation of the axial compression capacity can assist engineers toward an efficient design of circular concrete-filled steel tube (CCFST) columns, which are gaining popularity in diverse structural applications. This study proposes a novel methodology based on computational intelligence for estimating the compression capacity of CCFST. Accordingly, a conventional artificial neural network (ANN) is hybridized with a metaheuristic algorithm called the seeker optimization algorithm (SOA). Utilizing information such as the column's length, compressive strength of ultra-high-strength concrete, and the diameter, thickness, yield stress, and ultimate stress of the steel tube, the capacity of the column is predicted through non-linear calculations. In addition to the SOA, the future search algorithm (FSA) and social ski driver (SSD) are used as comparative benchmarks. The prediction results showed that the SOA-ANN can learn and predict the compression capacity pattern with high accuracy (relative error < 2.5% and correlation > 0.99). Also, this model outperformed both benchmark hybrids (i.e., FSA-ANN and SSD-ANN). Apart from accuracy, the configuration of the SOA-ANN is simpler owing to the smaller population recruited for the optimization task. An explicit formula for the proposed model is developed, which, owing to its observed efficiency, can be reliably applied to CCFST columns for the early estimation of the compression capacity.

**Keywords:** CCFST columns; axial compression capacity; composite structures; neural network; seeker optimization algorithm



**Citation:** Hu, P.; Aghajaninefah, H.; Anvari, A.; Nehdi, M.L. Combining Artificial Neural Network and Seeker Optimization Algorithm for Predicting Compression Capacity of Concrete-Filled Steel Tube Columns. *Buildings* **2023**, *13*, 391. <https://doi.org/10.3390/buildings13020391>

Academic Editor: Andreas

Lampropoulos

Received: 24 December 2022

Revised: 13 January 2023

Accepted: 25 January 2023

Published: 1 February 2023



**Copyright:** © 2023 by the authors. Licensee MDPI, Basel, Switzerland. This article is an open access article distributed under the terms and conditions of the Creative Commons Attribution (CC BY) license (<https://creativecommons.org/licenses/by/4.0/>).

## 1. Introduction

The world of engineering has witnessed significant advances in computational and evaluative methods during the past decades. It has enabled scholars of different domains to develop sophisticated tools/programs towards enhancing their scientific capabilities [1–3]. Civil engineering is one of these fields that comprises a wide variety of subjects from material-related analysis such as concrete [4,5] to safety of structures [6]. Civil engineers have successfully applied various experimental [7] and numerical [8] methods for solving problems such as dealing with seismic events [9]. For this purpose, they need to profoundly investigate the behavior of different parts of structures such as beams and columns for design purposes.

Circular concrete-filled steel tube (CCFST) columns are fundamental structural elements that are broadly used because of their compressive strength [10–12]. Hence, analyzing the axial compression capacity (ACC) of these elements has been the primary aim of many studies that has been fulfilled using various numerical and analytical methodologies.

Yu, et al. [13], for example, presented a unified formulation for designing hollow and solid polygonal CCFST columns. As for analytical approaches, Lai, et al. [14] developed a path-dependent stress-strain method for analyzing the behavior of CCFST columns. The accuracy of the model was finally accepted with respect to the accommodation between the observed and modeled load-strain curves. A similar methodology was tested by Chen, et al. [15] for concrete confined by fiber-reinforced polymer and corresponding CCFST columns. An ABAQUS-based numerical method was suggested by Zhang, et al. [16] for estimating the residual capacity of CCFST stub columns subjected to axial compression with a combined freeze situation. The model was verified by comparison with the experiment. Based on the executed sensitivity analysis, they professed that the influence of section size can be disregarded in calculations.

Toward more convenient and more efficient analysis, machine learning methods have recently been replaced with conventional models in many fields of research [17–19]. There is a wide variety of these models such as gene expression programming (GEP) [20], adaptive neuro-fuzzy inference system (ANFIS) [21], and multivariate adaptive regression splines [22] that have been effectively applied to problems related to the CCFST columns. Ho and Le [23] investigated the feasibility of a regression model for analyzing the ultimate load of CCFST columns by taking into account the variability propagated to the response. Tran, et al. [24] applied an artificial neural network (ANN) for analyzing the ACC of the CCFST columns. Utilizing the results of a series of finite element analyses, they could establish a neural relationship between the ACC and effective parameters. The resulting model was finally presented in the form of a graphical user interface. In a similar study by Nguyen, et al. [25], the feasibility of the ANN was proved for this purpose. Cosgun, et al. [26] conducted a comparison among some popular machine-learning methods including the ANN, random forest (RF), support-vector machines (SVM), and multiple linear regression (MLR), and showed that the ANN can present a more accurate approximation of the ultimate axial load carried by a CCFST.

Optimization algorithms are iterative techniques that aim to find the optimal solution to a problem. Defining the problem in a mathematical form, an optimization technique tries to minimize the cost function by improving the solution consecutively [27–30]. Sarir, et al. [31] conducted a comparison between a tree-based GEP and an ANN technique trained by particle swarm optimization (PSO). The accuracy assessment showed the higher capacity of the tree-GEP model. In the next phase of the study, they employed a whale optimization algorithm (WOA) for achieving the maximum bearing capacity of the CCFST columns. The findings revealed that the WOA can have significant contribution to the mentioned task.

In combination with machine learning, these algorithms can play the role of training strategies that tune the internal parameters (e.g., weights and biases). Nguyen, et al. [32] coupled an ANN with step secant algorithm (OSS) to create a surrogate hybrid model for analyzing the bearing capacity of rectangular CCFST columns. Likewise, Mai, et al. [33] tuned a radial basis ANN with firefly algorithm (FFA) and achieved significant improvements (around 52%) with respect to the basic model. Another application of the PSO can be found in the research by Nguyen, et al. [34]. They combined the PSO with an ANN and compared it with several benchmark techniques. According to the findings, the suggested hybrid performs the best and can efficiently predict the compressive strength of CCFST columns. Sine cosine algorithm (SCA) is another viable optimization technique that has recently been developed. Lyu, et al. [35] synthesized this algorithm with support vector regression (SVR) for estimating the ACC of the CCFST columns. Their results showed that the proposed SCA-SVR model can predict the ACC with significantly higher accuracy compared to a typical ANN, RF, and MLR. In detail, the correlation of the SVR model increased from 0.6603 to 0.9849 as the effect of the SCA algorithm. Ngo and Le [36] developed and tested a comparable hybrid model but with grey wolf optimization (GWO) instead of SCA. The results showed a more reliable understanding of the intelligent approaches relative to conventional empirical ones. Tran, et al. [37] used interior-point (IP) algorithm

to improve the performance of the ANN in predicting the ACC of elliptical CFST columns. Comparison of the results (e.g., correlation coefficients 0.983 vs. 0.938) showed that the IP-ANN is superior to the conventional version of this method. They also professed that this model can be efficient due to eliminating some costly experiments.

It is a well-accepted fact that such indirect evaluations can be of great interest to design engineers, due to the easiness of implementation and reducing the cost of civil engineering projects [38]. The successful performance of the metaheuristic optimization in various prediction problems [39,40] addresses the main motivation of this study to test the efficiency of novel hybrids in the field of ACC modeling. Although some previous studies have used metaheuristic techniques for training models like ANFIS, [41,42], training of the ANN can be more investigated. In this study, this task is assigned to seeker optimization algorithm (SOA), future search algorithm (FSA), and social ski-driver (SSD) which are among the potential metaheuristic optimizers. The algorithms are coupled with an ANN to tune its parameters for predicting the ACC of the CCFST column with ultra-high-strength concrete (UHSC). The models are also compared to previous literature to address the most capable one for practical applications.

## 2. Materials and Methods

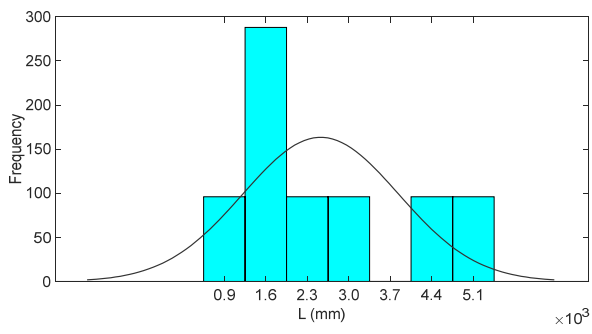
### 2.1. Data Provision

Data, as is known, provide the analyzable material for a data-mining system. In other words, the system acquires knowledge by exploring the relationship between the provided data. In this work, the target parameter is the ACC of the CCFST column with UHSC. Hence, the models seek to realize the dependency of this parameter on its influencing factors (i.e., input parameters). Since the basic network of this study is a neural network, a highly nonlinear relationship is supposed to be established. This relationship takes the effect of several input parameters simultaneously and calculates the ACC through a feed-forward strategy.

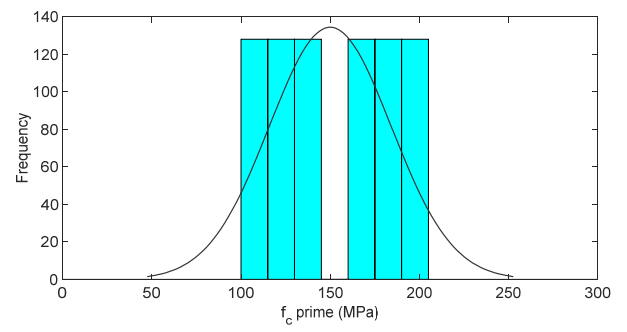
Based on the existing dataset created by Tran, Thai and Nguyen [24], six input parameters affect the ACC of the CCFST column. The length of column ( $L$ ), the compressive strength of UHSC ( $f'_c$ ), as well as four characteristics of the steel tube including diameter ( $D$ ), thickness ( $t$ ), yield stress ( $f_y$ ), and ultimate stress ( $f_u$ ). Figure 1a–g depicts a histogram for each of these input parameters. The values of  $L$ ,  $D$ ,  $t$ ,  $f_y$ ,  $f_u$ , and  $f'_c$  range in [900.0, 4800.0] mm, [300.0, 600.0] mm, [6.0, 30.0] mm, [235.0, 460.0] MPa, [360.0, 540.0] MPa, and [100.0, 200.0] MPa, with skewness values equal to 0.51, 0.00, 0.73, 0.42,  $-0.28$ , and 0.00, respectively. Also, the minimum and maximum ACC values are 8016.3 and 75,051.6 N with an average 30,185.3 N and skewness 0.55.

Zheng, Jin, Jiang, Moradi, Khadimallah and Moayedı [42] performed an importance assessment on this dataset using the random forest technique. According to their results,  $D$  and  $f'_c$  play the most important role in predicting the ACC, whereas  $f_u$  and  $L$  were characterized with the lowest importance values.

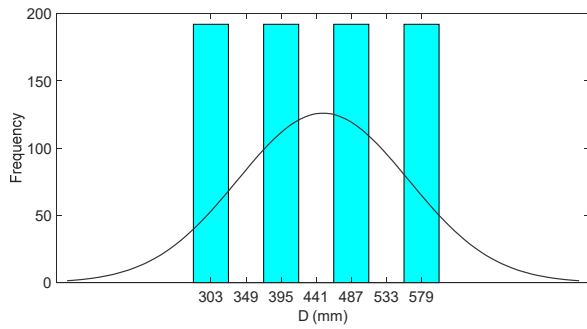
It was explained that the knowledge of an intelligent model is obtained after analyzing appropriate data. In more detail, only one group of data is dedicated to this objective. A smaller part of data are set aside to be used afterwards for assessing the quality of the acquired knowledge. It evaluates the prediction capability of the trained network when new conditions are imposed. These two groups are named training and testing datasets. In this work, a total of 768 records are available, out of which 614 records form the training dataset, and the remaining 154 records are selected as testing data; noting that a random selection is considered for this purpose. As is seen, the ratio of 80:20 is considered for this division which is a well-accepted ratio for such works.



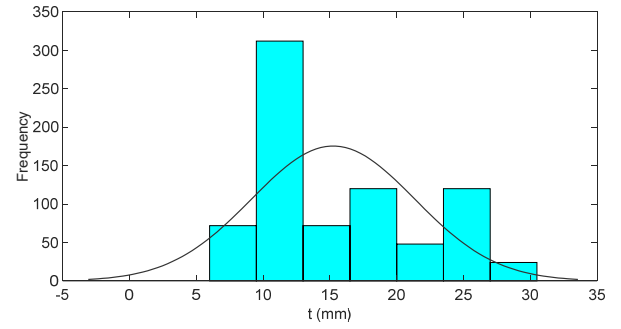
(a)



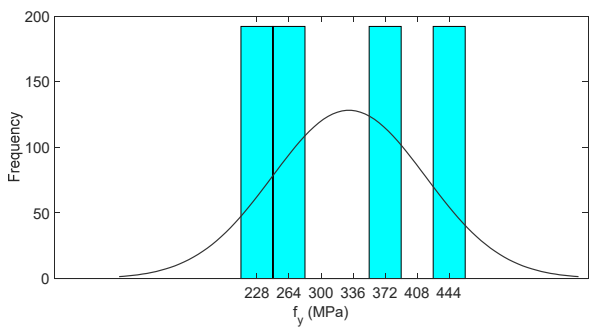
(b)



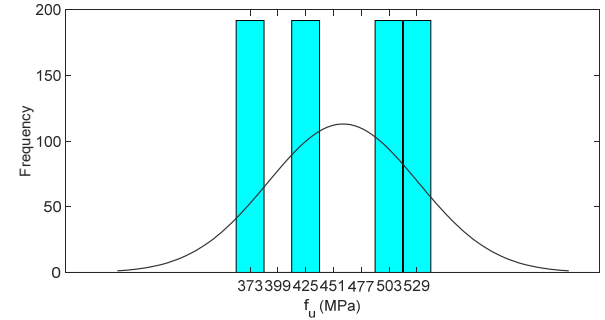
(c)



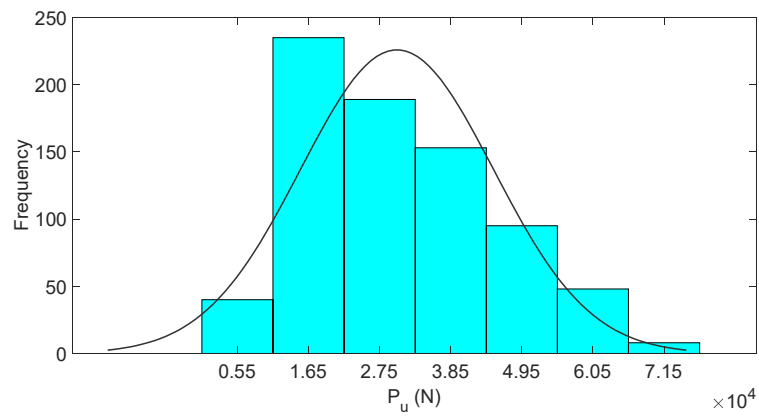
(d)



(e)



(f)



(g)

Figure 1. The frequency analysis of the input and target values.

## 2.2. The SOA

The SOA was introduced by Dai, et al. [43] as a stochastic approach for numerical optimization. The basis of this algorithm is human searching, and due to this, it was later renamed human group optimization. This algorithm has shown high convergence speed and good search efficacy for many applications [44].

The agents in this algorithm are called seekers. A neighborhood is defined for each agent for sharing social information. For each seeker  $I$  at time step  $t$ , two vectors of search direction and step length are defined as follows:

$$\vec{d}_i(t) = [d_{i1}, d_{i2}, \dots, d_{iD}], \quad (1)$$

$$\vec{\lambda}_t(t) = [\lambda_{t1}, \lambda_{t2}, \dots, \lambda_{tD}], \quad (2)$$

where  $\lambda_{ij}(t) \geq 0$  and  $d_{ij} \in \{-1, 0, 1\}$  ( $i = 1, 2, \dots, N_{pop}$  (population size) and  $j = 1, 2, \dots, D$  (dimension of problem)). Equation (3) shows how the  $j^{\text{th}}$  element of position of the seeker  $i$  is updated.

$$x_{ij}(t+1) = x_{ij}(t) + d_{ij} \lambda_{ij}, \quad (3)$$

Like many other search algorithms, the local minimum could be an important issue to the SOA algorithm. It is because subpopulations perform a search by using their knowledge. To overcome this issue, an inter-subpopulation learning method is devised for the algorithm. In this method, a binomial crossover operator performs to combine the two least-fitted positions of each subpopulation with the best-fitted position pertaining to each of the other two subpopulations. Equation (4) expresses this process.

$$x_{k_n, j, \text{worst}} = \begin{cases} x_{mj, \text{best}} & \text{if } R_j \leq 0.5 \\ x_{k_n, j, \text{worst}} & \text{else, } \end{cases} \quad j = 1, 2, \dots, D, \quad (4)$$

where  $x_{k_n, j, \text{worst}}$  denotes the  $j^{\text{th}}$  element of the  $n^{\text{th}}$  least-fitted position in the  $k^{\text{th}}$  subpopulation. Likewise,  $x_{mj, \text{best}}$  denotes the  $j^{\text{th}}$  element of the best-fitted position in the  $m^{\text{th}}$  subpopulation. Also,  $R_j$  is a random number uniformly placed within  $[0, 1]$  [45,46].

## 2.3. The FSA

Elsisi [47] developed the FSA based on the imitative behavior of individuals taken for improving the life quality. The population is accordingly defined as some nations which are sought by a person for his/her comfortable life. Unlike many existing algorithms in which the population is once generated and the best individual is detected after a long time, the FSA refreshes the irregular population at each iteration [48]. In this algorithm, a random population is first generated based on the below equation:

$$S(k, :) = L_b + (U_b - L_b) \times \text{rand}(1, D), \quad (5)$$

where  $S$  stands for the solution,  $D$  is the dimension of the space (i.e., the number of countries),  $k$  represents the present solution. Also, the lower and upper boundaries are represented by  $L_b$  and  $U_b$ , respectively.

The objective functions of the initial individuals are considered as the local solutions (LSs) and the best-fitted one is deemed as the global solution (GS). Both LS and GS are used during optimization using the FSA algorithm. Equation (6) expresses the exploitation phase of the algorithm which uses the LS of each country.

$$S(k, :)_L = (LS(k, :) - S(k, :)) \times \text{rand}(), \quad (6)$$

The exploration phase is then performed as shown in Equation (7). The GS is used in this step.

$$S(k, :)_G = (GS - S(k, :)) \times \text{rand}(), \quad (7)$$

By knowing the locally and globally persons across the world, one may decide to change the life as given in Equation (8).

$$S(k, :) = S(k, :) + S(k, :)_L + S(k, :)_G, \quad (8)$$

Equation (9) shows how the solutions are updated for modifying the initial population.

$$S(k, :) = GS + (GS - LS(k, :)) \times rand(), \quad (9)$$

This process is iteratively repeated and stops when the algorithm meets one convergence/stopping criterion [48]

#### 2.4. The SSD

This algorithm was proposed by Tharwat and Gabel [49] for optimizing the parameters of the SVM model. The SSD is drawn on the idea of different optimization algorithms. The search scheme of this method is a simulation of the downhill path taken by ski-drivers. Having  $n$  as the dimension of the problem,  $R^n$  shows the space in which the agents take position ( $X_i$ ). Like other optimization techniques, the cost function is calculated with respect to the agents' positions. Similar to the PSO technique, among different positions that are obtained for an agent, the best one is stored and is compared to the next positions [50]. Another simulated strategy that is embedded in the SSD algorithm is the movement of agents toward a mean global solution ( $M_i$ ). Referring to the grey wolf optimizer algorithm [51], the  $M_i$  is calculated as the average of three outstanding solutions ( $X_a$ ,  $X_b$ , and  $X_c$ ):

$$M_i^t = \frac{X_a + X_b + X_c}{3}, \quad (10)$$

In the SSD algorithm, the agents update their position using a velocity term as follows:

$$X_i^{t+1} = X_i^t + V_i^t, \quad (11)$$

in which the velocity of the  $i$ th agent is represented by  $V_i$ . Equation (12) expresses the calculation of  $V_i^{t+1}$ .

$$V_i^{t+1} = \begin{cases} c \cos(r_1)(P_i^t - X_i^t) + \cos(r_1)(M_i^t - X_i^t) & \text{if } r_2 > 0.5 \\ c \sin(r_1)(P_i^t - X_i^t) + \sin(r_1)(M_i^t - X_i^t) & \text{if } r_2 \leq 0.5 \end{cases} \quad (12)$$

where  $r_1$  and  $r_2$  are random values randomly generated in the range  $[0, 1]$  and  $P_i$  represents the best solution found so far. In addition,  $c$  is defined by Equation (13) to establish a balance between exploration and exploitation.

$$c^{t+1} = \beta c^t, \quad (13)$$

In the above equation,  $t$  stands for the iteration and  $\beta$  is a reducing factor that ranges from 0 to 1. Thus, the value of  $c$  goes toward 0 as  $t$  approaches the maximum number. Regarding the sine and cosine functions used in Equation (12), the moving strategy of this algorithm is not straightforward (unlike the GWO and PSO). It enables the agents to have a more diversified search path (i.e., higher exploration ability), however, in a guided way [49].

### 3. Results and Discussion

Analyzing the parameters of the materials used in the construction sector has been widely explored [52–54]. Following previous efforts for evaluating different structural units (e.g., foundation [55], beams [56], and frames [57]), this study offers new methodologies for approximating the capacity of the CCFST columns.

Evaluating the results consists of accuracy assessment using different indicators. It can be done by a calculation of prediction error and correlation. In the present study, the

three famous indices of RMSE, mean absolute error (MAE), and mean absolute percentage error (MAPE) are responsible for representing the error, and the correlation between the simulation outputs and expected  $P_{us}$  is calculated by the Pearson correlation coefficient ( $R_p$ ). Having  $ACC_{i_{expected}}$  and  $ACC_{i_{simulated}}$  as the  $i$ th ( $i = 1, 2, \dots, N$ ) observed and estimated values of the ACC, respectively, the formulations of these accuracy indicators are expressed as follows:

$$RMSE = \sqrt{\frac{1}{N} \sum_{i=1}^N [(ACC_{i_{expected}} - ACC_{i_{simulated}})]^2}, \quad (14)$$

$$MAE = \frac{1}{N} \sum_{i=1}^N |ACC_{i_{expected}} - ACC_{i_{simulated}}|, \quad (15)$$

$$MAPE = \frac{1}{N} \sum_{i=1}^N \left| \frac{ACC_{i_{expected}} - ACC_{i_{simulated}}}{ACC_{i_{expected}}} \right| \times 100, \quad (16)$$

$$R_p = \frac{\sum_{i=1}^N (ACC_{i_{simulated}} - \overline{ACC}_{simulated})(ACC_{i_{expected}} - \overline{ACC}_{expected})}{\sqrt{\sum_{i=1}^N (ACC_{i_{simulated}} - \overline{ACC}_{simulated})^2} \sqrt{\sum_{i=1}^N (ACC_{i_{expected}} - \overline{ACC}_{expected})^2}} \quad (17)$$

### 3.1. Parameter Optimization

In this work, all coding and implementations are carried out in the MATLAB environment. A neural network can be the skeleton of hybrid models, when the second incorporator plays the role of the training strategy [58,59]. Three hybrid models are tested for estimating the ACC of the CCFST column with UHSC. In each model, one metaheuristic algorithm, i.e., SOA, FSA, and SSD, is responsible for training the ANN. In this process, the network has two to-be-optimized parameters, namely weight and bias.

To calculate the exact number of weights and biases, it is necessary to know the general body of a neural network that partly corresponds to the used dataset. An ANN has a minimum of three layers. In the first layer, the neurons receive the input data. Hence, there are six neurons in the first layer (same as the number of input parameters). The second layer (also known as a hidden layer) concerns with main calculations and its number of neurons is experimentally determined to be five in this study. It is worth mentioning that a series of trial-and-error efforts were performed to support this decision. Finally, the unique neuron in the output layer is responsible for producing the final output (i.e., the ACC). Considering the connection between the input and hidden neurons, the created network has  $(6 \times 5 =)$  30 weights in the first part plus  $(5 \times 1 =)$  5 weights providing connections for the hidden and output neurons. In addition, there are six bias terms: five for hidden neurons and one for the output neuron. All in all, the ANN has 41 to-be-optimized parameters that should be properly adjusted by the trainer. Besides, the activation function of the hidden and output layers are Tansig and Purelin, respectively.

In each of the proposed models, i.e., SOA-ANN, FSA-ANN, and SSD-ANN, the metaheuristic algorithm goes through the search space and finds the optimal solution. It then reconstructs the ANN to predict the ACC using new weights and biases. This strategy is recursively implemented until the given condition is satisfied. In this work, a total of 1000 iterations are considered for the SOA, FSA, and SSD to have enough chance for optimizing their ANN. However, such algorithms have an important parameter, called population size, which can highly affect the quality of the solution. To solve this issue, the used algorithms are tried with different population sizes and their performances are compared to obtain the most accurate optimization. The criterion for evaluating the solutions is the RMSE calculated for both training and testing data. The results are shown in Table 1. As is seen, among the population sizes of 10, 25, 50, 100, 200, 300, 400, and 500, the lowest error of the SOA, FSA, and SSD has resulted for 100, 400, and 400, respectively.

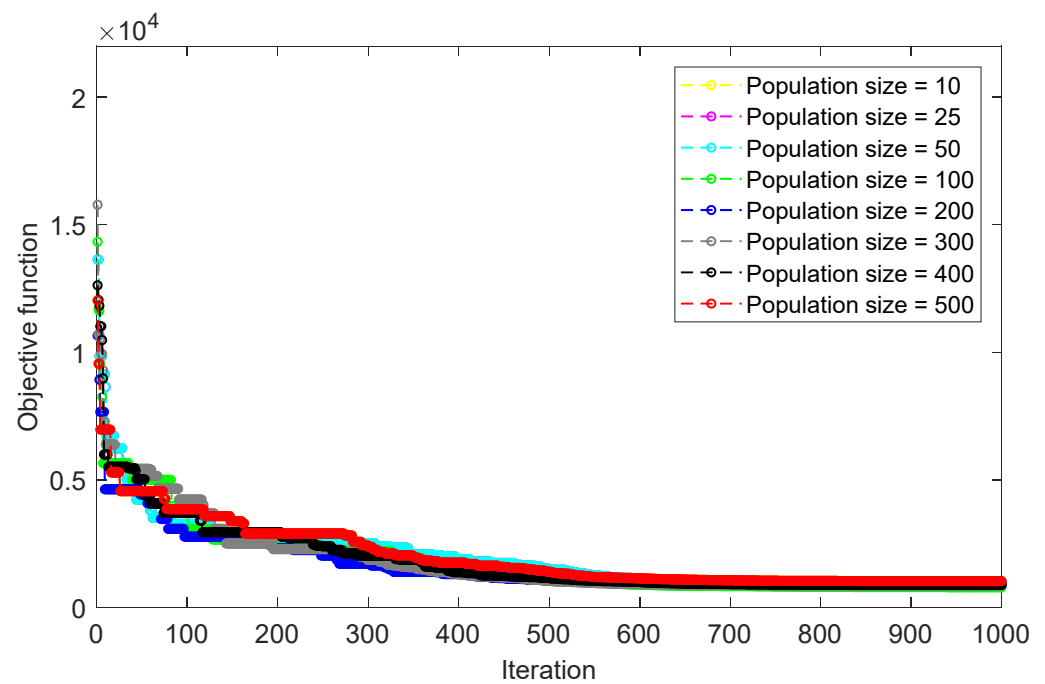
**Table 1.** Computed errors for different population sizes.

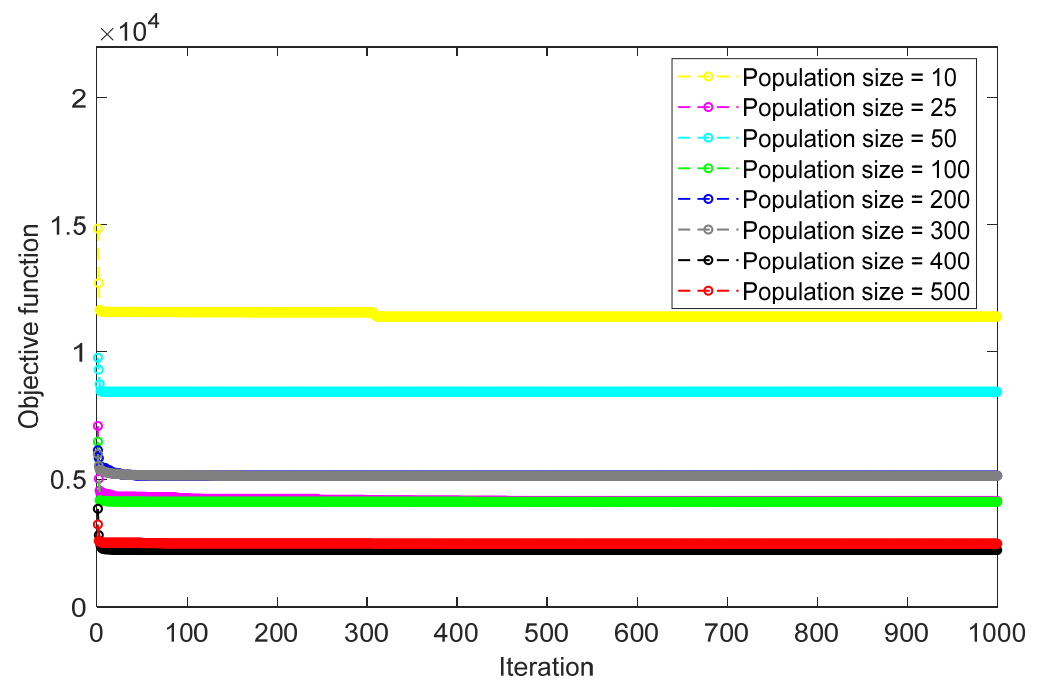
Population Size	Error (RMSE)					
	SOA		FSA		SSD	
	Train	Test	Train	Test	Train	Test
10	1025.3611	1112.7001	11,392.7308	12,078.6674	9342.3668	9225.4253
25	1004.0163	1049.8834	4145.1873	4244.6568	6810.4859	7444.0207
50	1004.0163	1049.8834	8435.5850	8679.0653	7559.0509	7667.1607
100	790.1621	825.3149	4109.1313	4184.6332	5773.8329	5380.2117
200	913.7759	971.8556	5140.9042	4832.3346	5413.4324	5092.9420
300	839.1691	938.2552	5136.5219	4562.0366	5611.5035	5533.1326
400	880.9083	951.6036	2215.2954	2136.6979	2614.6768	2604.5897
500	1025.3611	1112.7001	2468.9317	2742.0072	3855.7082	3459.6554
Minimum RMSE	790.1621	825.3149	2215.2954	2136.6979	2614.6768	2604.5897

Figure 2a–c illustrate the corresponding optimization curves. As is known, an optimization curve illustrates how the solution found by the algorithm is improving over iterations. As is seen, the used algorithms show completely different behavior in finding the optimal solution for the ANN. Another noticeable point is the distinction between the results of large and small population sizes. It supports the necessity of having such efforts toward finding an appropriate representative of the model.

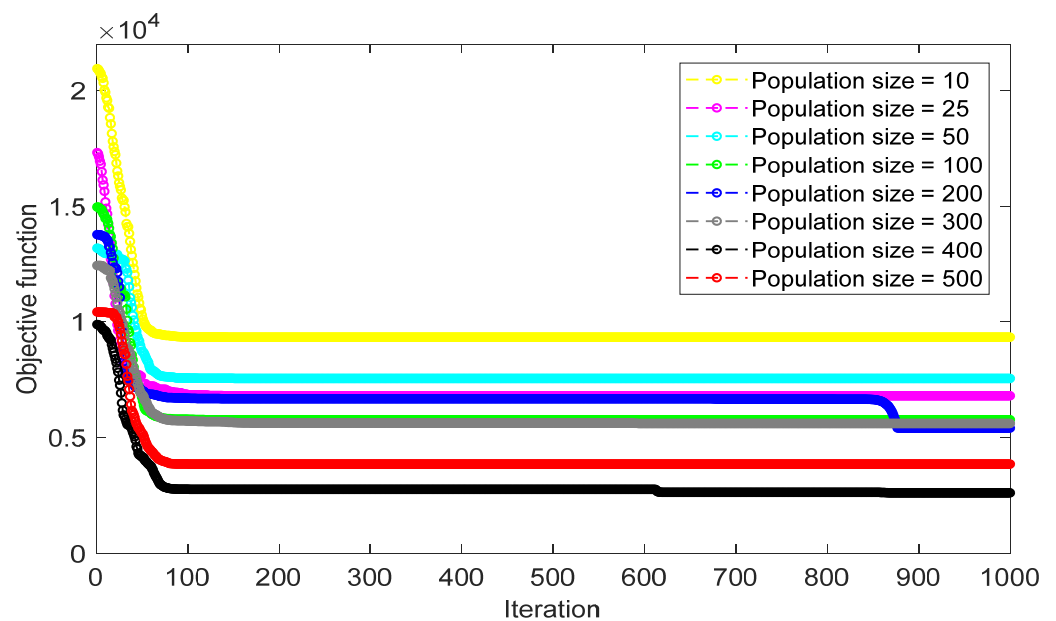
### 3.2. Prediction Results and Comparison

This section presents the results of the used models in predicting the ACC. First, the results of the training phase are statistically evaluated. Figure 3 depicts the error chart for 614 training samples. The error on the  $y$ -axis is the exact difference between the pair  $P_{u_{i_{expected}}}$  and  $P_{u_{i_{simulated}}}$  ( $i = 1, 2, \dots, 614$ ). Needless to say, the data on the line  $y = 0$  represent ideal predictions where the error is zero.

**(a)** SOA-MLP**Figure 2.** Cont.



(b) FSA-MLP



(c) SSD-ANN

**Figure 2.** Optimization curves of the implemented (a) SOA-ANN, (b) FSA-ANN, and (c) SSD-ANN.

According to the obtained RMSEs, 790.1621, 2215.2954, and 2614.6768 for the SOA-ANN, FSA-ANN, and SSD-ANN, respectively, all three models could acquire an acceptable understanding of the ACC behavior. This result can be similarly indicated by the MAE values of 571.1356, 1673.6446, and 1971.9976. Moreover, based on very low relative errors 2.2656%, 6.2182%, and 7.9524%, as well as high  $R_p$  values 0.99862, 0.98909, and 0.98522, it can be deduced that the training process has been satisfactorily carried out by all three algorithms.

However, referring to the same assessment, the superiority of the SOA algorithm can be inferred. The solution provided by this algorithm is of higher accuracy because the created ANN produces more accurate outputs. After that, the training process supervised

by the FSA was more promising than the SSD. In other words, the weights and biases found by the FSA could construct a more powerful neural network.

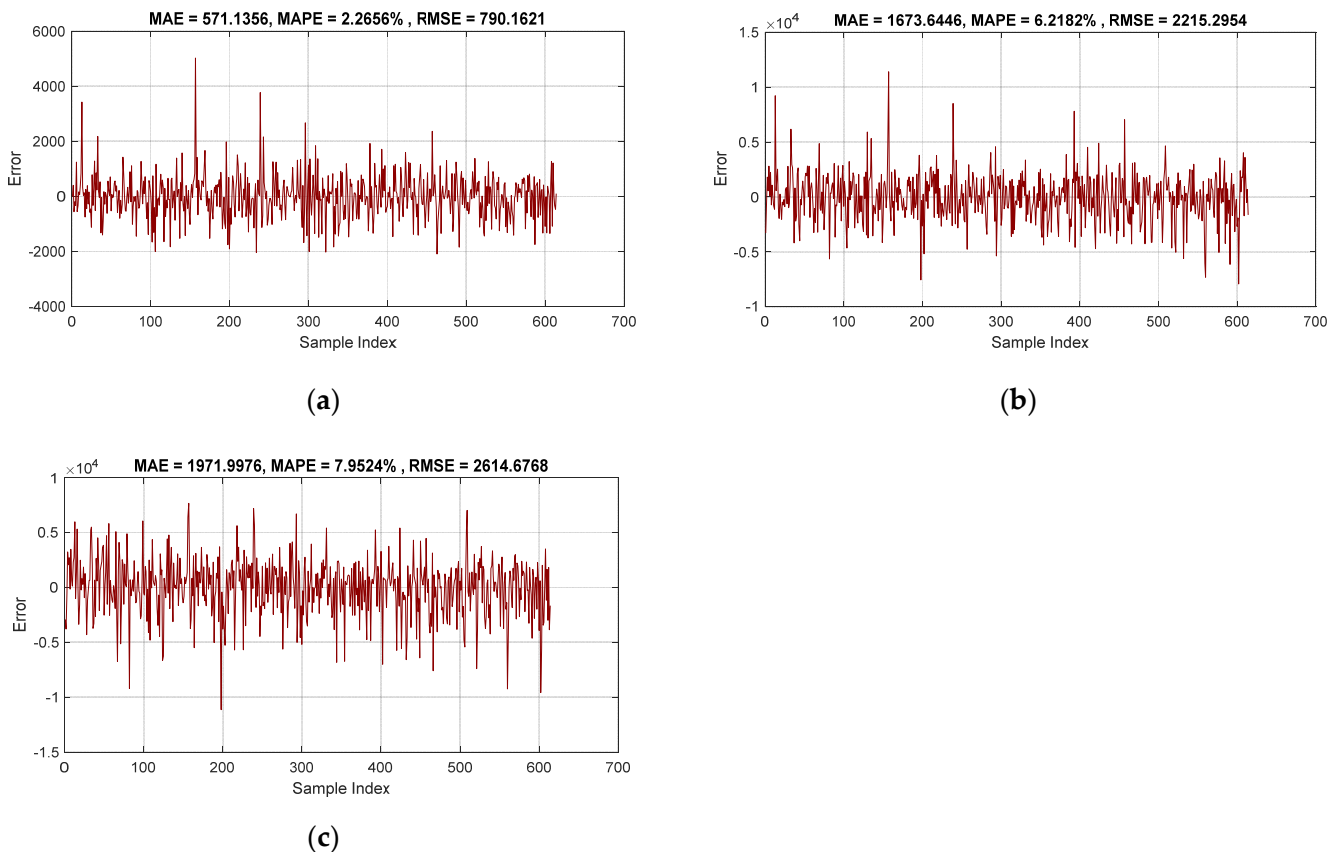


**Figure 3.** The pure training errors obtained by the (a) SOA-ANN, (b) FSA-ANN, and (c) SSD-ANN.

In the second phase of evaluation, the testing dataset is concerned. The trained SOA-ANN, FSA-ANN, and SSD-ANN predicted the ACC for 154 new conditions of CCFSTC with UHSC. Having the expected values, the agreement between the outputs and targets reflects the quality of prediction. Figure 4 is presented to show this concept. In such figures, the ideal prediction occurs when all data are settled on the line  $y = x$ , which gives an  $R_p = 1$ . In this case, the  $R_p$ s were 0.99836, 0.98896, and 0.98435. Accordingly, the results of all three models have a nice correlation with expected values. The calculated RMSEs were 825.3149, 2136.6979, and 2604.5897 which give a tolerable range of error. As for the MAEs, the calculated values were 633.4302, 1662.8879, and 2016.4144 which account for 2.4802%, 6.1011%, and 8.3695% relative error (i.e., MAPE).

### 3.3. Comparison and Further Assessment

From the above results, it can be deduced that all three models presented a reliable prediction of the ACC. It means that by providing the information of  $L$ ,  $D$ ,  $t$ ,  $f_y$ ,  $f_u$ , and  $f_c'$ , a close-to-reality analysis of the behavior of CCFST columns can be expected. Going more deeply into the networks, the weights and biases suggested by the SOA, FSA, and SSD could create a generalizable pattern.

From the comparison point of view, there was no discrepancy between the training and testing results; meaning that the model with a higher quality training achieved a higher quality prediction. Hence, the ANN trained by the SOA was the most accurate network, followed by the FSA and SSD. Having the results of both phases altogether, the SOA emerged as a more powerful optimization technique compared to the FSA and SSD. Likewise, the FSA surpassed the SSD. However, it should be noted that this conclusion is derived for the objective of this study.

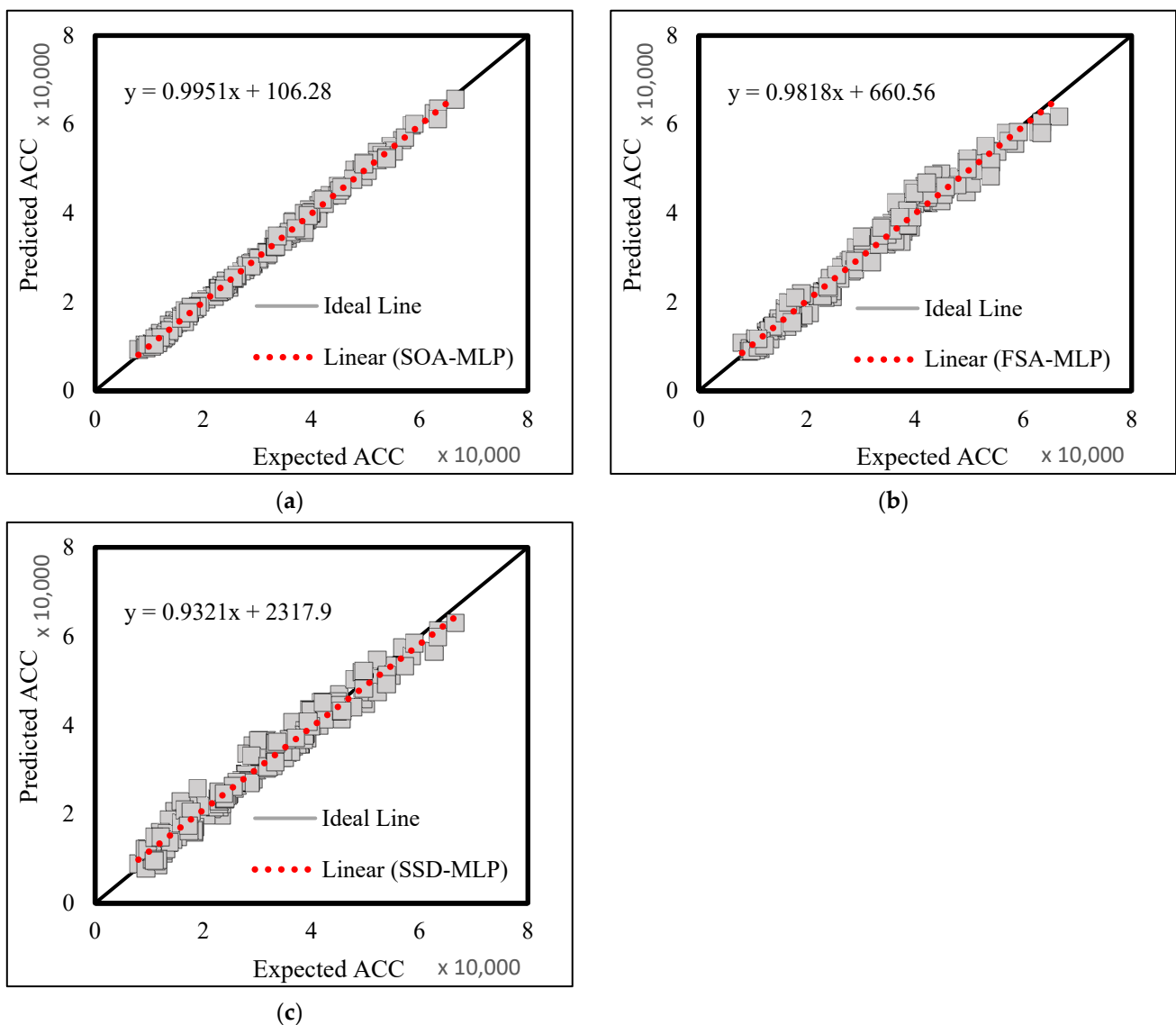


**Figure 4.** The scatter charts of the testing results for (a) SOA-ANN, (b) FSA-ANN, and (c) SSD-ANN.

The achievement of this study is also compared to previous works that have applied intelligent combined models to the same dataset. In studies by Karimi Sharafshadeh, Ketabdari, Azarsina, Amiri and Nehdi [41] and Zheng, Jin, Jiang, Moradi, Khadimallah and Moayedi [42], several metaheuristic techniques (including equilibrium optimization (EO) [60], grey wolf optimization (GWO) [51], Harris hawk optimizer (HHO) [61], earthworm algorithm (EWA) [62], salp swarm algorithm (SSA) [63], and teaching learning-based optimization (TLBO) [64]) incorporated the ANFIS model to similarly predict the ACC. As shown in Table 2, the accuracy criteria of six models are compared to the ones obtained for the SOA-ANN, FSA-ANN, and SSD-ANN in this study. At a glance, all accuracy criteria of the SOA-ANN model show lower error and higher correlation for this model compared to all eight models. These results indicate that a significant improvement is obtained in the prediction accuracy of the ACC by using the SOA algorithm.

### 3.4. An Explicit Formula

Producing and presenting an explicit formula is the last objective of this study. As explained, the configuration of an ANN is a layered non-linear combination of weights and biases influenced by an activation function. On the other hand, since the SOA-ANN was the most accurate model, it was decided to present this model in the form of a two-part

formula. Equations (18) and (19) correspond to the calculations performed in the hidden and output layer of the ANN, respectively. As is seen, each of the five neurons in the hidden layer produces an output expressed by  $Z_i$  ( $i = 1, 2, \dots, 5$ ). These values are later used by the output neuron to produce the ACC. In Equation (18), Tansig is the activation function of the neurons that causes the non-linearity of the simulation. This function is expressed in Equation (20).

**Table 2.** Computed values of RMSE, MAE, MAPE,  $R_p$  in this study and previous literature.

Study	Models	Network Results							
		Training Phase				Testing Phase			
		RMSE	MAPE	MAE	$R_p$	RMSE	MAPE	MAE	$R_p$
This study	SOA-ANN	790.16	2.27	571.14	0.99862	825.31	2.48	633.43	0.99836
	FSA-ANN	2215.30	6.22	1673.64	0.98909	2136.70	6.10	1662.89	0.98896
	SSD-ANN	2614.68	7.95	1972.00	0.98522	2604.59	8.37	2016.41	0.98435
[41]	EWA-ANFIS	3984.79	12.41	3085.06	0.96436	4033.84	12.92	12.92	0.96106
	SSA-ANFIS	2950.36	10.39	2296.06	0.98055	2874.74	10.62	10.62	0.98004
	TLBO-ANFIS	2923.11	10.29	2282.50	0.98092	2854.81	10.49	10.49	0.98037
[42]	EO-ANFIS	1275.95	4.05	956.77	0.99640	1346.17	4.18	1022.85	0.99564
	GWO-ANFIS	2944.91	10.37	2291.41	0.98062	2872.76	10.59	2324.19	0.98006
	HHO-ANFIS	1422.89	4.55	1071.82	0.99551	1492.50	4.89	1184.65	0.99462

$$\begin{bmatrix} Z_1 \\ Z_2 \\ Z_3 \\ Z_4 \\ Z_5 \end{bmatrix} = \text{Tansig} \left( \left( \begin{bmatrix} 0.963 & -0.800 & -0.523 & 0.509 & 0.590 & 0.950 \\ 1.113 & -0.274 & 0.320 & -1.026 & -0.823 & -0.453 \\ -1.017 & -0.660 & -0.347 & -0.960 & 0.783 & -0.476 \\ -0.975 & 1.342 & 0.400 & -0.319 & 0.137 & 0.566 \\ 0.147 & -0.707 & -1.099 & -0.500 & 0.069 & 1.170 \end{bmatrix} \begin{bmatrix} D \\ L \\ t \\ f_y \\ f_u \\ f'_c \end{bmatrix} \right) + \begin{bmatrix} -1.831 \\ -0.915 \\ 0.000 \\ -0.915 \\ 1.831 \end{bmatrix} \right), \quad (18)$$

$$\text{ACC} = -0.841 \times Z_1 + 0.555 \times Z_2 + 0.217 \times Z_3 - 0.614 \times Z_4 - 0.570 \times Z_5 - 0.342, \quad (19)$$

$$\text{Tansig}(x) = \frac{2}{1 + e^{-2x}} - 1, \quad (20)$$

#### 4. Conclusions

Analyzing the axial compression capacity of concrete-filled steel tube columns is substantial in structural engineering. Many recent works have reported successful applications of machine learning models, especially metaheuristic-optimized ones, for this purpose. This work suggested and tested a hybrid model (i.e., a neural network supervised by seeker optimization algorithm) for predicting the ACC of the CCFST column. According to the training results, the predictive model could effectively learn the behavior of the CCFST column given the column characteristics. Evaluating the testing results proved the high generalizability of this approach in dealing with unseen specimens. In addition, several accuracy assessment criteria were applied to compare the proposed SOA-ANN to two similar ANN hybrids (i.e., FSA-ANN and SSD-ANN), as well as six ANFIS hybrid models from previous studies (i.e., EWA-ANFIS, SSA-ANFIS, TLBO-ANFIS, EO-ANFIS, GWO-ANFIS, and HHO-ANFIS). The results revealed that the SOA-ANN performed the task with higher accuracy. Hence, it can be a reliable alternative to traditional approaches (e.g., finite elements) for designing the CCFST columns with respect to their compression capacity. However, more algorithms and prediction strategies are suggested to be tried in future relevant works towards improving the discovered solutions.

**Author Contributions:** P.H.: Data Curation, Formal Analysis, Investigation, Software, Visualization, Writing—Original Draft; H.A.: Data Curation, Formal Analysis, Investigation, Software, Visualization, Writing—Original Draft; A.A.: Data Curation, Formal Analysis, Investigation, Software, Visualization, Writing—Original Draft; M.L.N.: Conceptualization, Funding Acquisition, Methodology, Project Administration, Resources, Writing—Review and Editing. All authors have read and agreed to the published version of the manuscript.

**Funding:** This work was supported by Research on Key Hydraulic Technology of Bionic Fishway Construction, Grant/Award Number: CX2017Z19; Countermeasures and action plan for stability and sustainability protection of water ecosystem in the Three Gorges Reservoir Area.

**Data Availability Statement:** The data used in this study is created by Tran, Thai and Nguyen [24] and is available in that study.

**Conflicts of Interest:** The authors declare no conflict of interest.

## References

1. Ijaz, Z.; Zhao, C.; Ijaz, N.; Rehman, Z.U.; Ijaz, A. Novel application of Google earth engine interpolation algorithm for the development of geotechnical soil maps: A case study of mega-district. *Geocarto Int.* **2022**, 1–21. [[CrossRef](#)]
2. Zhang, C.; Kordestani, H.; Shadabfar, M. A combined review of vibration control strategies for high-speed trains and railway infrastructures: Challenges and solutions. *J. Low Freq. Noise Vib. Act. Control* **2022**, 14613484221128682. [[CrossRef](#)]
3. Huang, H.; Li, M.; Yuan, Y.; Bai, H. Experimental Research on the Seismic Performance of Precast Concrete Frame with Replaceable Artificial Controllable Plastic Hinges. *J. Struct. Eng.* **2023**, 149, 04022222. [[CrossRef](#)]
4. Zhang, Z.; Liang, G.; Niu, Q.; Wang, F.; Chen, J.; Zhao, B.; Ke, L. A Wiener degradation process with drift-based approach of determining target reliability index of concrete structures. *Qual. Reliab. Eng. Int.* **2022**, 38, 3710–3725. [[CrossRef](#)]
5. Deng, E.-F.; Zhang, Z.; Zhang, C.-X.; Tang, Y.; Wang, W.; Du, Z.-J.; Gao, J.-P. Experimental study on flexural behavior of UHPC wet joint in prefabricated multi-girder bridge. *Eng. Struct.* **2023**, 275, 115314. [[CrossRef](#)]
6. Zhang, Z.; Li, W.; Yang, J. Analysis of stochastic process to model safety risk in construction industry. *J. Civ. Eng. Manag.* **2021**, 27, 87–99. [[CrossRef](#)]
7. Fu, Q.; Gu, M.; Yuan, J.; Lin, Y. Experimental study on vibration velocity of piled raft supported embankment and foundation for ballastless high speed railway. *Buildings* **2022**, 12, 1982. [[CrossRef](#)]
8. Gu, M.; Cai, X.; Fu, Q.; Li, H.; Wang, X.; Mao, B. Numerical Analysis of Passive Piles under Surcharge Load in Extensively Deep Soft Soil. *Buildings* **2022**, 12, 1988. [[CrossRef](#)]
9. Zhang, C.; Ali, A. The advancement of seismic isolation and energy dissipation mechanisms based on friction. *Soil Dyn. Earthq. Eng.* **2021**, 146, 106746.
10. Fam, A.; Qie, F.S.; Rizkalla, S. Concrete-filled steel tubes subjected to axial compression and lateral cyclic loads. *J. Struct. Eng.* **2004**, 130, 631–640. [[CrossRef](#)]
11. Chitawadagi, M.V.; Narasimhan, M.C.; Kulkarni, S. Axial strength of circular concrete-filled steel tube columns—DOE approach. *J. Constr. Steel Res.* **2010**, 66, 1248–1260. [[CrossRef](#)]
12. Liang, J.; Lin, S.; Li, W.; Liu, D. Axial compressive behavior of recycled aggregate concrete-filled square steel tube stub columns strengthened by CFRP. *Structures* **2021**, 29, 1874–1881. [[CrossRef](#)]
13. Yu, M.; Zha, X.; Ye, J.; Li, Y. A unified formulation for circle and polygon concrete-filled steel tube columns under axial compression. *Eng. Struct.* **2013**, 49, 1–10. [[CrossRef](#)]
14. Lai, M.; Song, W.; Ou, X.; Chen, M.; Wang, Q.; Ho, J. A path dependent stress-strain model for concrete-filled-steel-tube column. *Eng. Struct.* **2020**, 211, 110312. [[CrossRef](#)]
15. Chen, P.; Wang, Y.; Liu, C. Confinement path-dependent analytical model for FRP-confined concrete and concrete-filled steel tube subjected to axial compression. *Compos. Struct.* **2018**, 201, 234–247. [[CrossRef](#)]
16. Zhang, T.; Lyu, X.; Yu, Y. Prediction and analysis of the residual capacity of concrete-filled steel tube stub columns under axial compression subjected to combined freeze–thaw cycles and acid rain corrosion. *Materials* **2019**, 12, 3070. [[CrossRef](#)]
17. Liao, L.; Du, L.; Guo, Y. Semi-supervised SAR target detection based on an improved faster R-CNN. *Remote Sens.* **2021**, 14, 143. [[CrossRef](#)]
18. Zhan, C.; Dai, Z.; Soltanian, M.R.; de Barros, F.P. Data-Worth Analysis for Heterogeneous Subsurface Structure Identification With a Stochastic Deep Learning Framework. *Water Resour. Res.* **2022**, 58, e2022WR033241. [[CrossRef](#)]
19. Rehman, Z.; Khalid, U.; Ijaz, N.; Mujtaba, H.; Haider, A.; Farooq, K.; Ijaz, Z. Machine learning-based intelligent modeling of hydraulic conductivity of sandy soils considering a wide range of grain sizes. *Eng. Geol.* **2022**, 311, 106899. [[CrossRef](#)]
20. Nour, A.I.; Güneş, E.M. Prediction model on compressive strength of recycled aggregate concrete filled steel tube columns. *Compos. Part B Eng.* **2019**, 173, 106938. [[CrossRef](#)]
21. Le, T.-T.; Phan, H.C. Prediction of ultimate load of rectangular CFST columns using interpretable machine learning method. *Adv. Civ. Eng.* **2020**, 2020, 8855069. [[CrossRef](#)]

22. Avci-Karatas, C. Prediction of ultimate load capacity of concrete-filled steel tube columns using multivariate adaptive regression splines (MARS). *Steel Compos. Struct.* **2019**, *33*, 583–594.
23. Ho, N.X.; Le, T.-T. Effects of variability in experimental database on machine-learning-based prediction of ultimate load of circular concrete-filled steel tubes. *Measurement* **2021**, *176*, 109198. [[CrossRef](#)]
24. Tran, V.-L.; Thai, D.-K.; Nguyen, D.-D. Practical artificial neural network tool for predicting the axial compression capacity of circular concrete-filled steel tube columns with ultra-high-strength concrete. *Thin-Walled Struct.* **2020**, *151*, 106720. [[CrossRef](#)]
25. Nguyen, M.-S.T.; Thai, D.-K.; Kim, S.-E. Predicting the axial compressive capacity of circular concrete filled steel tube columns using an artificial neural network. *Steel Compos. Struct.* **2020**, *35*, 415–437.
26. Cosgun, C.; Cosgun, O.; Sadeghian, R.; Aram, S. Prediction of Ultimate Load Capacity of Concrete-Filled Steel Tubes with Circular Sections under Axial Load by Using Predictive Analytics Methods. In Proceedings of the 2020 International Conference on Computational Science and Computational Intelligence (CSCI), Las Vegas, NV, USA, 16–18 December 2020; pp. 664–667.
27. Arandian, B.; Iraj, A.; Alaei, H.; Keawsawasvong, S.; Nehdi, M.L. White-Tailed Eagle Algorithm for Global Optimization and Low-Cost and Low-CO<sub>2</sub> Emission Design of Retaining Structures. *Sustainability* **2022**, *14*, 10673. [[CrossRef](#)]
28. Mehrabi, M.; Pradhan, B.; Moayedi, H.; Alamri, A. Optimizing an adaptive neuro-fuzzy inference system for spatial prediction of landslide susceptibility using four state-of-the-art metaheuristic techniques. *Sensors* **2020**, *20*, 1723. [[CrossRef](#)]
29. Moayedi, H.; Mehrabi, M.; Bui, D.T.; Pradhan, B.; Foong, L.K. Fuzzy-metaheuristic ensembles for spatial assessment of forest fire susceptibility. *J. Environ. Manag.* **2020**, *260*, 109867. [[CrossRef](#)]
30. Ashrafian, A.; Hamzehkolaei, N.S.; Dwijendra, N.K.A.; Yazdani, M. An Evolutionary Neuro-Fuzzy-Based Approach to Estimate the Compressive Strength of Eco-Friendly Concrete Containing Recycled Construction Wastes. *Buildings* **2022**, *12*, 1280. [[CrossRef](#)]
31. Sarir, P.; Chen, J.; Asteris, P.G.; Armaghani, D.J.; Tahir, M. Developing GEP tree-based, neuro-swarm, and whale optimization models for evaluation of bearing capacity of concrete-filled steel tube columns. *Eng. Comput.* **2021**, *37*, 1–19. [[CrossRef](#)]
32. Nguyen, Q.H.; Ly, H.-B.; Tran, V.Q.; Nguyen, T.-A.; Phan, V.-H.; Le, T.-T.; Pham, B.T. A novel hybrid model based on a feedforward neural network and one step secant algorithm for prediction of load-bearing capacity of rectangular concrete-filled steel tube columns. *Molecules* **2020**, *25*, 3486. [[CrossRef](#)] [[PubMed](#)]
33. Mai, S.H.; Seghier, M.E.A.B.; Nguyen, P.L.; Jafari-Asl, J.; Thai, D.-K. A hybrid model for predicting the axial compression capacity of square concrete-filled steel tubular columns. *Eng. Comput.* **2022**, *38*, 1205–1222. [[CrossRef](#)]
34. Nguyen, M.-S.T.; Trinh, M.-C.; Kim, S.-E. Uncertainty quantification of ultimate compressive strength of CCFST columns using hybrid machine learning model. *Eng. Comput.* **2022**, *38*, 2719–2738. [[CrossRef](#)]
35. Lyu, F.; Fan, X.; Ding, F.; Chen, Z. Prediction of the Axial Compressive Strength of Circular Concrete-Filled Steel Tube Columns using Sine Cosine Algorithm-Support Vector Regression. *Compos. Struct.* **2021**, *273*, 114282. [[CrossRef](#)]
36. Ngo, N.-T.; Le, H.A. Integration of support vector regression and grey wolf optimization for estimating the ultimate bearing capacity in concrete-filled steel tube columns. *Neural Comput. Appl.* **2021**, *33*, 8525–8542. [[CrossRef](#)]
37. Tran, V.-L.; Jang, Y.; Kim, S.-E. Improving the axial compression capacity prediction of elliptical CFST columns using a hybrid ANN-IP model. *Steel Compos. Struct.* **2021**, *39*, 319–335.
38. Zhao, Y.; Moayedi, H.; Bahiraei, M.; Foong, L.K. Employing TLBO and SCE for optimal prediction of the compressive strength of concrete. *Smart Struct. Syst.* **2020**, *26*, 753–763.
39. Mehrabi, M.; Moayedi, H. Landslide susceptibility mapping using artificial neural network tuned by metaheuristic algorithms. *Environ. Earth Sci.* **2021**, *80*, 804. [[CrossRef](#)]
40. Moayedi, H.; Mehrabi, M.; Kalantar, B.; Abdullahi Mu'azu, M.; Rashid, A.S.A.; Foong, L.K.; Nguyen, H. Novel hybrids of adaptive neuro-fuzzy inference system (ANFIS) with several metaheuristic algorithms for spatial susceptibility assessment of seismic-induced landslide. *Geomat. Nat. Hazards Risk* **2019**, *10*, 1879–1911. [[CrossRef](#)]
41. Karimi Sharafshadeh, B.; Ketabdari, M.J.; Azarsina, F.; Amiri, M.; Nehdi, M.L. New Fuzzy-Heuristic Methodology for Analyzing Compression Load Capacity of Composite Columns. *Buildings* **2023**, *13*, 125. [[CrossRef](#)]
42. Zheng, Y.; Jin, H.; Jiang, C.; Moradi, Z.; Khadimallah, M.A.; Moayedi, H. Analyzing behavior of circular concrete-filled steel tube column using improved fuzzy models. *Steel Compos. Struct.* **2022**, *43*, 625–637.
43. Dai, C.; Chen, W.; Song, Y.; Zhu, Y. Seeker optimization algorithm: A novel stochastic search algorithm for global numerical optimization. *J. Syst. Eng. Electron.* **2010**, *21*, 300–311. [[CrossRef](#)]
44. Tuba, M.; Brajevic, I.; Jovanovic, R. Hybrid seeker optimization algorithm for global optimization. *Appl. Math. Inf. Sci.* **2013**, *7*, 867. [[CrossRef](#)]
45. Dai, C.; Chen, W.; Li, L.; Zhu, Y.; Yang, Y. Seeker optimization algorithm for parameter estimation of time-delay chaotic systems. *Phys. Rev. E* **2011**, *83*, 036203. [[CrossRef](#)] [[PubMed](#)]
46. Dai, C.; Chen, W.; Zhu, Y.; Jiang, Z.; You, Z. Seeker optimization algorithm for tuning the structure and parameters of neural networks. *Neurocomputing* **2011**, *74*, 876–883. [[CrossRef](#)]
47. Elsis, M. Future search algorithm for optimization. *Evol. Intell.* **2019**, *12*, 21–31. [[CrossRef](#)]
48. Janamala, V.; Kumar, U.K.; Pandraju, T.K.S. Future search algorithm for optimal integration of distributed generation and electric vehicle fleets in radial distribution networks considering techno-environmental aspects. *SN Appl. Sci.* **2021**, *3*, 464. [[CrossRef](#)]
49. Tharwat, A.; Gabel, T. Parameters optimization of support vector machines for imbalanced data using social ski driver algorithm. *Neural Comput. Appl.* **2020**, *32*, 6925–6938. [[CrossRef](#)]
50. Poli, R.; Kennedy, J.; Blackwell, T. Particle swarm optimization. *Swarm Intell.* **2007**, *1*, 33–57. [[CrossRef](#)]

51. Mirjalili, S.; Mirjalili, S.M.; Lewis, A. Grey wolf optimizer. *Adv. Eng. Softw.* **2014**, *69*, 46–61. [[CrossRef](#)]
52. Shi, T.; Liu, Y.; Zhao, X.; Wang, J.; Zhao, Z.; Corr, D.J.; Shah, S.P. Study on mechanical properties of the interfacial transition zone in carbon nanofiber-reinforced cement mortar based on the PeakForce tapping mode of atomic force microscope. *J. Build. Eng.* **2022**, *61*, 105248. [[CrossRef](#)]
53. Shi, T.; Liu, Y.; Hu, Z.; Cen, M.; Zeng, C.; Xu, J.; Zhao, Z. Deformation Performance and Fracture Toughness of Carbon Nanofiber-Modified Cement-Based Materials. *ACI Mater. J.* **2022**, *119*, 119–128.
54. Ma, Z.; Shen, J.; Wang, C.; Wu, H. Characterization of sustainable mortar containing high-quality recycled manufactured sand crushed from recycled coarse aggregate. *Cem. Concr. Compos.* **2022**, *132*, 104629. [[CrossRef](#)]
55. Chen, J.; Tong, H.; Yuan, J.; Fang, Y.; Gu, R. Permeability prediction model modified on kozeny-carman for building foundation of clay soil. *Buildings* **2022**, *12*, 1798. [[CrossRef](#)]
56. Huang, Y.; Zhang, W.; Liu, X. Assessment of diagonal macrocrack-induced debonding mechanisms in FRP-strengthened RC beams. *J. Compos. Constr.* **2022**, *26*, 04022056. [[CrossRef](#)]
57. Huang, H.; Li, M.; Yuan, Y.; Bai, H. Theoretical analysis on the lateral drift of precast concrete frame with replaceable artificial controllable plastic hinges. *J. Build. Eng.* **2022**, *62*, 105386. [[CrossRef](#)]
58. Moayedi, H.; Mehrabi, M.; Mosallanezhad, M.; Rashid, A.S.A.; Pradhan, B. Modification of landslide susceptibility mapping using optimized PSO-ANN technique. *Eng. Comput.* **2019**, *35*, 967–984. [[CrossRef](#)]
59. Nguyen, H.; Mehrabi, M.; Kalantar, B.; Moayedi, H.; Abdullahi, M.A.M. Potential of hybrid evolutionary approaches for assessment of geo-hazard landslide susceptibility mapping. *Geomat. Nat. Hazards Risk* **2019**, *10*, 1667–1693. [[CrossRef](#)]
60. Faramarzi, A.; Heidarinejad, M.; Stephens, B.; Mirjalili, S. Equilibrium optimizer: A novel optimization algorithm. *Knowl.-Based Syst.* **2020**, *191*, 105190. [[CrossRef](#)]
61. Heidari, A.A.; Mirjalili, S.; Faris, H.; Aljarah, I.; Mafarja, M.; Chen, H. Harris hawks optimization: Algorithm and applications. *Future Gener. Comput. Syst.* **2019**, *97*, 849–872. [[CrossRef](#)]
62. Wang, G.-G.; Deb, S.; dos Santos Coelho, L. Earthworm optimisation algorithm: A bio-inspired metaheuristic algorithm for global optimisation problems. *Int. J. Bio-Inspired Comput.* **2018**, *12*, 1–22. [[CrossRef](#)]
63. Mirjalili, S.; Gandomi, A.H.; Mirjalili, S.Z.; Saremi, S.; Faris, H.; Mirjalili, S.M. Salp Swarm Algorithm: A bio-inspired optimizer for engineering design problems. *Adv. Eng. Softw.* **2017**, *114*, 163–191. [[CrossRef](#)]
64. Rao, R.V.; Savsani, V.J.; Vakharia, D. Teaching–learning-based optimization: A novel method for constrained mechanical design optimization problems. *Comput.-Aided Des.* **2011**, *43*, 303–315. [[CrossRef](#)]

**Disclaimer/Publisher’s Note:** The statements, opinions and data contained in all publications are solely those of the individual author(s) and contributor(s) and not of MDPI and/or the editor(s). MDPI and/or the editor(s) disclaim responsibility for any injury to people or property resulting from any ideas, methods, instructions or products referred to in the content.